Journal of The Electrochemical Society

Characterization of a Regenerative Hydrogen-Vanadium Fuel Cell Using an Experimentally Validated Unit Cell Model

Characterization of a Regenerative Hydrogen-Vanadium Fuel Cell Using an Experimentally Validated Unit Cell Model

C. A. Pino-Muñoz,[z] B. K. Chakrabarti, V. Yufit, and N. P. Brandon

Department of Earth Science and Engineering, Imperial College London, London SW7 2AZ, United Kingdom

A hydrogen-vanadium electrochemical system was characterized using extensive experimental tests at different current densities and flow rates of vanadium electrolyte. The maximum peak power density achieved was 2840 W m^{-2} along with a limiting current density of over 4200 A m^{-2}. The cycling performance presented a stable coulombic efficiency over 51 cycles with a mean value of 99.8%, while the voltage efficiency decreased slowly over time from a value of 90.3% to 87.0%. The capacity loss was of 5.6 A s per cycle, which could be related to crossover of ionic species and liquid water. A unit cell model, previously proposed by the authors, was modified to include the effect of species crossover and used to predict the cell potential. Reasonable agreement between the model simulations and the experimental charge-discharge data was observed, with Normalized Root-Mean-Square Errors (NRMSEs) within the range of 0.8–5.3% and 2.9–19.0% for charge and discharge, respectively. Also, a good degree of accuracy was observed in the simulated trend of the polarization and power density, with NRMSEs of 3.1% and 1.0%, and 1.1% and 1.9%, for the operation at a flow rate of vanadium electrolyte of 100 and 50 mL min^{-1}, respectively, while the voltage efficiency during the cycling test were estimated within a Root-Mean-Square Error (RMSE) of 1.9%. A study of the effect of the component properties on the cell potential was carried out by means of a model sensitivity analysis. The cell potential was sensitive to the cathodic transfer coefficient and the cathode porosity, which are directly related to the cathodic overpotential through the Butler-Volmer equation and the cathodic ohmic overpotential. It was recognized that a kinetic study for the cathodic reaction is needed to obtain more reliable kinetic parameters at practical vanadium concentrations, as well as reliable microstructural parameters of carbon electrodes.

 [DOI: 10.1149/2.0211914jes]

Manuscript submitted May 24, 2019; revised manuscript received August 23, 2019. Published October 17, 2019.

The rapid growth in the deployment of renewable energy sources such as wind, solar and others, has increased interest in electrochemical energy storage.[1,2] All-Vanadium Redox Flow Batteries (VRFBs), having the ability to decouple power and energy, with limited impact of cross-mixing, have drawn increasing attention from researchers.[3–6] Amongst VRFB limitations are the relatively low solubility and stability of vanadium ions in sulphuric acid solutions, and the high cost of vanadium-based electrolytes and membranes.[2–4,7] Electrolyte imbalance due to species crossover across the membrane can also be a challenge. To reduce cost dependency with regards to vanadium, new systems that employ only half of the vanadium required in a VRFB have been proposed and demonstrated.[3] Alternatively, hybrid-type Redox Flow Batteries (RFBs) such as hydrogen-halogen, have gained interest due to their fast reversible kinetics and the facile separation of crossover species if present.[8,9] However, significant safety concerns related to high vapor pressures, including leakage or release of toxic fumes exist for cells utilizing chlorine or bromine.[3,10] A Regenerative Hydrogen-Vanadium Fuel Cell (RHVFC) benefits from the advantages of the mixed liquid-gas RFBs, and reduces the overall system cost by utilizing only half of the vanadium electrolyte required for a VRFB. Still, a precious metal catalyst is required at the anode for the Hydrogen Oxidation/Evolution Reaction (HOR/HER). Capacity loss in the RHVFC due to crossover of catholyte solution to the anodic half-cell can be regained by collecting any crossover of vanadium electrolyte and returning it to the vanadium tank,[11] while capacity loss due to self-discharge or side reactions[12] could be regained by similar methods to those used in conventional VRFBs. The RHVFC was first proposed and demonstrated by Yufit et al.,[11] with a peak performance of 114 mW cm^{-2} at 100% SOC. The RHVFC utilizes V(V) and V(IV) as the cathodic redox couple, and hydrogen and protons as the anodic redox couple. The cell structure generally contains a porous carbon layer for the cathode, a cation exchange membrane and a catalyzed porous carbon layer for the anode, along with serpentine or interdigitated flow fields.[9,11,13] Figure 1 shows the typical single-cell assembly for the hydrogen-vanadium system. During discharge, V(V) is reduced to V(IV) and H_2 is oxidized to H^+, while the reverse process occurs during charge and H_2 is produced. A study of the loss mechanisms of the RHVFC was introduced,[9] observing that the cathodic diffusion and ohmic losses are the largest contribution to the total polarization, and the possible adsorption of vanadium ions onto the platinum catalyst. The cathodic losses could be explained by the partial wettability of the cathode due to its hydrophobic nature and the need for heat-treatment.[14–16] More recently, a first modelling approximation of the various physico-chemical phenomena involved in a RHVFC was proposed and validated.[17] Mathematical modelling and simulation of electrochemical cells are used to relate operational conditions to performance, predict and rationalize experimental findings and to study performance optimization.[2,18] The model combines a series of differential and algebraic equations assuming a uniform spatial distribution of species concentrations.[17] The model formulation, i.e., a zero-dimensional approach, maintains simplicity in comparison to spatially distributed approaches in order to allow its practical use in system monitoring and design where the fast computational speed is essential. Despite the implemented simplifications, the unit cell model was able to describe the potential dynamics of a hydrogen-vanadium cell of 25 cm^2 electrode cross-sectional area. This cell presented, however, some limitations including high ohmic losses that made it difficult to extract the electrode overpotentials in the cell. As part of this unit cell model, a complete Nernst equation was proposed to estimate the cell Open Circuit Potential (OCP), along with a complete Butler-Volmer (BV) approach to describe the relationship between current density and overpotential at the cathode. Unlike previous VRFB models, this complete BV approach includes all active ionic species involved in the redox reaction at the cathode. Also recently, Dowd et al.[13] demonstrated an improved performance for the RHVFC, reaching a power density of 540 mW cm^{-2} when using a carbon nanotube cathode, thinner membranes, and interdigitated flow fields. They also presented a crossover study,[12] showing that Electrospun Blended Nanofiber (EBN) based membranes (Nafion/PVDF, 30–40 μm) were capable of reducing the crossover rates while maintaining similar performance in comparison to those shown by conventional Nafion membranes.

In this study, a characterization of the performance of the RHVFC is presented. This performance study is based on experimental data obtained using a cell of 5 cm^2 electrode cross-sectional area and simulations from a validated unit cell model. In the following section, we calibrate and validate the unit cell model, using experimental measurements of electrochemical impedance spectroscopy (EIS), OCP, single-cycle charge-discharge potential at galvanostatic operational mode, polarization curves and cycling. Then, a sensitivity analysis of

[z]E-mail: c.pino15@imperial.ac.uk

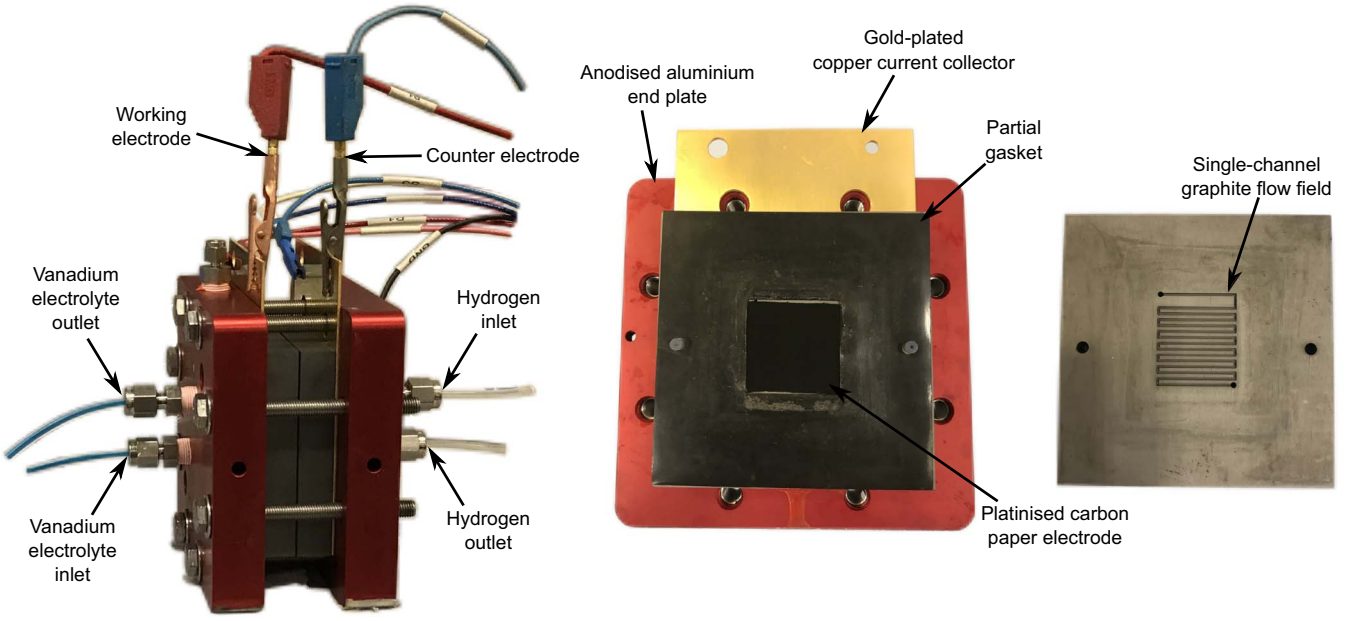

Figure 1. RHVFC system and its components.

the model is presented to study the influence of component properties, such as geometrical and material, on the performance of the cell.

RHVFC Unit Cell Model

The redox reactions that occur at the RHVFC electrodes are presented in Equations 1 and 2, and the overall cell reaction in Equation 3, where the charged species VO^{2+} and VO_2^+ represent the V(IV) and V(V) oxidation states, and E° is the standard potential with the subscripts "ca", "an" and "cell" referring to cathode, anode, and cell, respectively. In this work, the following commonly used convention has been applied, the cathode, which can equally be called the positive electrode, is the electrode where the reduction reaction occurs during the discharge of the battery. Therefore, the anode, which can equally be called the negative electrode, is the electrode where the oxidation reaction occurs during the discharge of the battery.

$$2VO_2^+ + 4H_3O^+ + 2e^- \underset{\text{charge}}{\overset{\text{discharge}}{\rightleftharpoons}} 2VO^{2+} + 6H_2O, \quad E^\circ_{ca} = 0.99\ \text{V vs. SHE} \tag{1}$$

$$H_2 + 2H_2O \underset{\text{charge}}{\overset{\text{discharge}}{\rightleftharpoons}} 2H_3O^+ + 2e^-, \quad E^\circ_{an} = 0\ \text{V vs. SHE} \tag{2}$$

$$2VO_2^+ + 2H_3O^+ + H_2 \underset{\text{charge}}{\overset{\text{discharge}}{\rightleftharpoons}} 2VO^{2+} + 4H_2O, \quad E^\circ_{cell} = 0.99\ \text{V vs. SHE} \tag{3}$$

A time dependent unit cell model previously introduced by the authors was used to model the RHVFC.[17] The domains considered in this unit cell model were: vanadium electrolyte tank, cathode, membrane, catalyst layer (CL), gas diffusion layer (GDL), and anode channel. General assumptions and simplifications taken are:

1. All domains are considered isothermal.
2. Electrolyte is considered incompressible, having constant density and viscosity.
3. Physical properties and mass and charge transfer properties are assumed isotropic and homogeneous in all the domains.
4. Unit activity coefficients are assumed for all species. However, an activity term is considered for the chemical dissociation of HSO_4^-, and a fitted global activity coefficient is considered for the estimation of OCP. Further explanation of this approach can be found in our previous work.[17]
5. The electrolytes and the membrane must maintain electroneutrality
   $\sum z_i c_i = 0$, for electrolytes
   $\sum z_i c_i + z_f c_f = 0$, for membrane.
6. Dilute solution approximation is considered for the conservation of species.
7. Gas evolution reactions in the cathode are neglected.
8. Side reactions are neglected.
9. Dissociation of bisulphate ions is assumed to reach equilibrium instantaneously.
10. Water balance at the cathode directly affects the catholyte tank volume.
11. Protons are the dominant charge carriers in the membrane.
12. Constant concentration of ionic species is assumed at the anode catalyst layer.

A number of parameters and properties were required to inform the unit cell model. Table I summarizes the geometrical properties and some of the material properties. A detailed explanation of the proposed model, stating equations, specific assumptions, limitations and capabilities of the model can be found in our previous work,[17] as well as any parameter value not included here. All physical property values are based on mean values reported in the literature. The parameters and variables mentioned throughout this work can be found in the List of Symbols section at the end of this document along with their respective units. Different mass transport and electrochemical processes were taken into account to formulate the mass conservation equations for all ionic species. Species balances were proposed for vanadium species (VO^{2+} and VO_2^+) and sulphuric acid species (H^+, HSO_4^- and SO_4^{2-}) at the cathode, and hydrogen as well as liquid and vapor water at the anode. Transport of protons, vanadium species and dissolved water was considered at the membrane.

In the present work, a water balance at the cathode and the effect of the crossover of ionic species was added to the previous model.[17] At the cathode, water is affected by the electrochemical reaction, the electro-osmotic drag and the diffusive transport through the membrane. The membrane ionic crossover is treated according to the modelling approach reported by Darling et al.[23] The molar flux of ionic species i, ($N_{i,m}$), can be expressed by the Nernst-Planck equation,[24] which represents the ionic transport due to diffusive, migration and convective fluxes, as shown in Equation 4. In this equation, c_i, $D_{i,m}$, z_i, and

Table I. Geometric and material properties for the electrodes, membrane and current collectors.

Parameter	Symbol	Value	Unit	Source
Thickness of vanadium electrode	l_{ca}	210×10^{-6}	m	Fuel cell store[19]
Thickness of hydrogen electrode	l_{an}	235×10^{-6}	m	Fuel cell store[20]
Thickness of membrane	l_m	127×10^{-6}	m	Fuel cell store[21]
Thickness of current collector	l_{cc}	0.0127	m	Scribner Associates[22]
Electronic conductivity of electrodes	σ_e	500	S m^{-1}	Estimated
Electronic conductivity of current collector	σ_{cc}	5000	S m^{-1}	Estimated (Figure 3)
Mean fiber diameter of vanadium electrode	d_f^{ca}	7.92×10^{-6}	m	Experimentally determined - ImageJ, Fiji
Mean pore diameter of vanadium electrode	d_p^{ca}	21.01×10^{-6}	m	Experimentally determined - InageJ, Fiji
Porosity of vanadium electrode	ε_{ca}	0.79/0.79	–	Experimentally determined - Avizo/TauFactor
Specific surface area of vanadium electrode	S_{ca}^{geo}	$4.29/1.44 \times 10^5$	m^2 m^{-3}	Experimentally determined - Avizo/TauFactor
Roughness factor of hydrogen electrode	R_{an}	200	m^2 m^{-2}	Assumed

$\mu_{i,m}$ are the concentration, diffusion coefficient, charge number and mobility of species i in the membrane, ϕ is the potential in the solution, v is the bulk velocity, F is the Faraday constant, and the superscript "m" refers to the membrane. The ion mobility can be eliminated as an independent parameter when using the Nernst-Einstein equation, $\mu_{i,m} = D_{i,m}/RT$, where R is the universal gas constant and T is the temperature.

$$N_{i,m} = -D_{i,m}\nabla c_i^m - z_i\mu_{i,m}Fc_i^m\nabla\phi + c_i^m v \quad [4]$$

Following the approach of Darling et al.[23] and assuming that protons are the main charge carrier in the membrane, the bulk velocity in the membrane was estimated considering the electro-osmotic and diffusive flow ($N_{w,m}$) by means of Equation 5. For the sake of simplicity, the transport of water was assumed to reach a steady state condition.[17] Additionally, the migration term in Equation 4 can be simplified by considering Ohm's law in the membrane as shown in Equation 6. By substituting Equations 5 and 6 in Equation 4, and performing the space integration for a constant current density subject to boundary conditions of concentration at each side of the membrane,[23] an expression for the ionic flux of species i through the membrane was obtained, as shown in Equation 7. Concentration of species at each side of the membrane can be specified as the concentration at the cathode (c_i^{ca}) and CL (c_i^{CL}). This flux was incorporated in the respective conservation equation for vanadium and sulphuric acid species. The term σ_m is the membrane conductivity, ξ_{drag} is the electro-osmotic drag coefficient, $\bar{c}_w$ is the mean concentration of water in the membrane ($c_w = \lambda\rho_{dm}/EW$, where λ is the water content, ρ_{dm} is the dry membrane density and EW is the equivalent molecular weight of the dry membrane), j is the applied current density, l_m is the membrane thickness, and D_w is the diffusion coefficient of water in the membrane.

$$N_{w,m} = \bar{c}_w v = \frac{\xi_{drag} j}{F} - D_w\frac{(c_w^{CL} - c_w^{ca})}{l_m} \quad [5]$$

$$j = -\sigma_m\nabla\phi \quad [6]$$

$$N_{i,m} = \frac{D_{i,m}c_i^{ca}}{l_m}\left(\frac{\zeta(e^{\zeta} - c_i^{CL}/c_i^{ca})}{e^{\zeta} - 1}\right)$$
$$\zeta = \left(\frac{z_i F}{\sigma_m RT} + \frac{\xi_{drag}}{\bar{c}_w D_{i,m}F}\right)jl_m - \frac{D_w}{D_{i,m}}\frac{(c_w^{CL} - c_w^{ca})}{\bar{c}_w} \quad [7]$$

It is a common assumption in models of all-vanadium systems to consider that all the concentrations of vanadium species at the opposite electrode are equal to zero due to self-discharge reactions at each electrode.[25] These self-discharge reactions supposedly take place instantaneously when vanadium species reach the opposite electrode and come in contact with other vanadium species.[23,26] In this work, possible side reactions[12] and self-discharge reactions are neglected, and therefore, the presence of ionic species at the anode catalyst layer could occur. This consideration coincides with what was observed after operating the cell and disassembling the Membrane Electrode Assembly (MEA), where a catholyte-like solution was found between the surface of the membrane and anode CL. For the sake of simplicity, a constant value of concentration of ionic species was considered at the anode CL (c_i^{CL}), allowing for transport through the membrane toward both electrodes which depends on the operating mode.

It is important to mention that a complete Nernst equation, whose detailed derivation from thermodynamic principles can be found in our previous work,[17] was used to calculate the OCP as shown in Equation 8. Here the species activities were substituted by concentrations, partial pressures and activity coefficients, by means of the activity definition ($a_i = \gamma_i c_i$) and Henry's law for hydrogen. This equation considers a global factor ($F_\gamma = \gamma_{VO_2^+}^{ca}\gamma_{H^+}^{ca}/\gamma_{VO^{2+}}^{ca}$), which was fitted to experimental OCP data, to account for neglected effects such as non-unitary activity coefficients.

$$E_{OCP} = E_{cell}^{\circ} + \frac{RT}{F}\ln\left(\frac{c_{VO_2^+}^{ca}c_{H^+}^{ca}(p_{H_2}^g)^{0.5}}{c_{VO^{2+}}^{ca}} \times \frac{\gamma_{VO_2^+}^{ca}\gamma_{H^+}^{ca}}{\gamma_{VO^{2+}}^{ca}}\right) \quad [8]$$

In the above equation, the term E_{OCP} is the open circuit potential, c_i^k and γ_i^k denote the bulk concentration and activity coefficient of species i in the domain k, and $p_{H_2}^g$ is the hydrogen pressure in the gaseous phase at the anode.

The operating cell potential, E_{cell}, was estimated considering the reversible OCP (E_{OCP}), ohmic overpotential (η_{ohm}) and electrode overpotentials for the cathode and anode (η_{ca} and η_{an}).[28] The different overpotentials were added to the OCP for charge operation and were subtracted for discharge operation, i.e., $E_{cell} = E_{OCP} \pm \eta_{ohm} \pm |\eta_{ca}| \pm |\eta_{an}|$. A complete Butler-Volmer (BV) approach is used to describe the overpotential of the cathode as given by Equation 9, considering the effect of the concentration of protons in the vanadium electrolyte. This overpotential approach estimates a total cathodic overpotential, including mass-transport limitation effects that are considered by the inequality of concentrations of species in the bulk and surface of the electrode. The applied current density can be obtained according to $j = S_{ca}V_{ca}j^{BV}/A_{ca}$, and the exchange current density was estimated from Equation 10, accounting for the effect of vanadium species and protons.

$$j^{BV} = j_0^{BV}\left[\left(\frac{c_{VO_2^+}^s}{c_{VO_2^+}}\right)\left(\frac{c_{H^+}^s}{c_{H^+}}\right)^2\exp\left(\frac{-\alpha_c F\eta_{ca}}{RT}\right) - \left(\frac{c_{VO^{2+}}^s}{c_{VO^{2+}}}\right)\exp\left(\frac{\alpha_a F\eta_{ca}}{RT}\right)\right] \quad [9]$$

In these equations, the terms j^{BV} and j_0^{BV} are the current density and exchange current density (current per unit active surface area of pore walls) of the cathode, respectively, α_c and α_a are the cathodic and anodic transfer coefficients for the vanadium redox reaction (Equation 1), k_{ca} is the rate constant, S_{ca} is the active specific surface area of the cathode (active surface area of pore walls per unit volume of electrode), and c_i^s is the surface concentration of species i at the liquid-solid interface of the electrode.

$$j_0^{BV} = Fk_{ca}\left(c_{VO^{2+}}\right)^{\alpha_c}\left(c_{VO_2^+}\right)^{\alpha_a}\left(c_{H^+}\right)^{2\alpha_a} \quad [10]$$

Table II. Experimental data sets measured in the 5 cm^2 area RHVFC.

Set	Test[a]	Current density[b]/A m^{-2}	Vanadium flow rate[c]/mL min^{-1}	Hydrogen flow rate[c]/mL min^{-1}
1	1st ch	100	100	100
2	EIS	0	100	100
3 - 9	ch-dis	100, 200, 300, 400, 500, 1000, 1500	100	100
10	PC	40:120:3880, 4040, 4200, 4360	100	100
11	1st ch	100	50	100
12	EIS	0	50	100
13 & 14	OCP	0	50	100
15 - 21	ch-dis	100, 200, 300, 400, 500, 1000, 1500	50	100
22	PC	40:120:3880, 4040, 4200, 4360	50	100
23	Cycling	700	50	30

[a]OCP: open circuit potential, ch-dis: charge-discharge, EIS: electrochemical impedance spectroscopy, PC: polarization/power curve.
[b]$j_1 : \Delta j : j_2$ refers to current densities from j_1 to j_2 with increments of Δj.
[c]Flow rates are given in mL min^{-1} in order to facilitate comparison. Flow rates of 100, 50 and 30 mL min^{-1} correspond to 1.6×10^{-6}, 8.3×10^{-7} and 5×10^{-7} m^3 s^{-1}, respectively.

The dependency of the cathodic rate constant with temperature can be expressed by an Arrhenius approach, as shown in Equation 11.

$$k_{ca} = k_{ca,ref} \exp\left(- \frac{F E^{\circ}_{ca,T_{ref}}}{R} \left[\frac{1}{T_{ref}} - \frac{1}{T} \right] \right) \quad [11]$$

Equation 9 considers the mass transport limitation effects, which increase at high current densities or extreme SOC conditions during cell charge and discharge.[17,29] The surface concentrations of species were evaluated by matching the rate of electrode reaction with the rate at which electro-active species are brought to the surface by mass transport.[30] These mass transport fluxes were assumed to be driven by a linear concentration gradient within a Nernst's diffusion layer (δ^{ca}), as described in Equation 12. Where D_i is the diffusion coefficient of species i in the vanadium electrolyte.

$$\begin{aligned} -\frac{D_{VO^{2+}}}{\delta^{ca}}(c_{VO^{2+}} - c^{s}_{VO^{2+}}) &= \frac{j^{BV}}{F} \\ \frac{D_{VO_2^{+}}}{\delta^{ca}}(c_{VO_2^{+}} - c^{s}_{VO_2^{+}}) &= \frac{j^{BV}}{F} \\ \frac{D_{H^{+}}}{\delta^{ca}}(c_{H^{+}} - c^{s}_{H^{+}}) &= 2\left(\frac{j^{BV}}{F}\right) \end{aligned} \quad [12]$$

For the anode, a Tafel-Volmer (TV) kinetic approach was considered as has been proposed by Kucernak and Zalitis (2016),[31] and given in Equation 13. This TV kinetic approach describes the current density-overpotential relation as independent of the pH, and only dependent on the hydrogen partial pressure and kinetic rate constants under near mass-transport free conditions. The coverage of hydrogen on the electrode surface ($\theta^{TV}_{H_{ad}}$) is also considered a function of the hydrogen pressure and the overpotential, as shown in Equation 14. It is assumed that the reaction is controlled by a single activation energy (E_{an})[31] and the effect of temperature is considered in Equation 16. The effect of liquid content in the CL by means of a liquid saturation term (s_{CL}) was added to this equation. The applied current density can be obtained according to $j = R_{an} j^{TV}$, where R_{an} is the roughness factor of the CL (active surface area of CL per unit cross-sectional area of electrode) and j^{TV} is the current density at operating conditions (current per unit area of the active surface area of CL).

$$\frac{j^{TV}}{k_{des}} = FZ\left(\theta^{TV}_{H_{ad}} e^{\beta f \eta_{an}} - B\left(1 - \theta^{TV}_{H_{ad}}\right) e^{-(1-\beta) f \eta_{an}}\right) \quad [13]$$

$$\begin{aligned} \theta^{TV}_{H_{ad}} = \Big[& 4B^2 + Z\left(e^{\beta f \eta_{an}} + B e^{-(1-\beta) f \eta_{an}}\right) \\ & - \Big[16B^2 + \left(Z\left(e^{\beta f \eta_{an}} + B e^{-(1-\beta) f \eta_{an}}\right)\right)^2 \\ & + 8BZ\left(B e^{\beta f \eta_{an}} + e^{-(1-\beta) f \eta_{an}}\right)\Big]^{0.5}\Big] / \left[4\left(B^2 - 1\right)\right] \end{aligned} \quad [14]$$

where,

$$B = \left(\frac{a_{H_2} k_{ad}}{k_{des}}\right)^{0.5}, \quad Z = \frac{k^{eq}_{V}}{k_{des}}, \quad f = \frac{F}{RT} \quad [15]$$

$$j^{TV} = (1 - s_{CL}) j^{TV,\varnothing} \exp\left(- \frac{E_{an}}{R} \left(\frac{1}{T} - \frac{1}{298.15} \right) \right) \quad [16]$$

In the above equations, the term β represents the transfer coefficient of the hydrogen redox reaction (Equation 2), k_{ad} and k_{des} are the adsorption and desorption rate constants of the Tafel reaction, k_V is the forward rate constant of the Volmer reaction, and a_{H_2} represents the activity of dissolved hydrogen, which is equivalent to the change in partial pressure of hydrogen.[31]

Experimental

Experimental data were collected to study the performance of the RHVFC. Galvanostatic tests were performed using a single cell (Scribner Associates) having a cross-sectional area of 5 cm^2 (height and width of 2.24×10^{-2} m), which is shown in Figure 1. The cell consisted of anodised aluminum end plates, gold-plated copper current collectors, graphite flow fields and the Membrane Electrode Assembly (MEA). The MEA contained a carbon paper electrode (Freudenberg H23, 210 μm) and a platinised carbon paper electrode (SGL 29BC, 235 μm, 0.3 mg cm^{-2} Pt loading), which were separated by a Nafion 115 membrane (127 μm). Single-channel serpentine graphite flow fields permitted to distribute the vanadium electrolyte, as well as the hydrogen gas, into the cell. A torque of 4 N m was applied to each of the 8 bolts used to compress the cell. For all experiments, a 0.8 M V(IV) electrolyte solution was prepared by dissolving 10.8 g of vanadium sulphate hydrate (Sigma-Aldrich) in 60 mL of 5 M H_2SO_4 solution (Fluka Analytical). Hydrogen was passed through the anode side at a constant flow rate, while a small glass reservoir was connected to the hydrogen outlet to collect any vanadium electrolyte crossover. A peristaltic pump (Cole Parmer) was used to circulate the vanadium electrolyte between the cell and the reservoir at a constant flow rate.

The galvanostatic tests were performed using a Bio-Logic potentiostat (VSP-300) running EC-Lab software. A summary of the operating conditions used in the experimental tests is presented in Table II. The flow rate of vanadium electrolyte was set to 50 or 100 mL min^{-1}, and the hydrogen flow rate to 100 mL min^{-1}. For all tests, the system was allowed to reach an upper cut-off potential of 1.4 V and a lower cut-off potential of 0.4 V. Electrochemical impedance spectroscopy (EIS) was carried out at OCP condition with a State Of Charge (SOC) of 100%. The EIS measurements were carried out after the first galvanostatic charge of fresh solution of vanadium electrolyte at a current density of 100 A m^{-2}. These EIS measurements were taken in galvanostatic mode with an AC current R.M.S value of 0.005 A over

a frequency range from 1 MHz to 100 mHz, and with 6 points per decade of frequency. The OCP behavior as a function of SOC was measured by charging or discharging the cell on a series of capacity steps at constant current density, and measuring OCP after each charging or discharging step. The cell SOC was calculated by comparing the experimental capacity with the maximum theoretical capacity, which was calculated considering the fresh solution preparation. Single-cycle charge-discharge tests were performed at constant current density in the range of 100–1500 A m^{-2}, with OCP measurements performed after galvanostatic charge or discharge mode. Polarization and power characteristic curves were obtained at an initial SOC of 100%, by applying steps of galvanostatic discharge at constant current density in the range of 40 to 4200 A m^{-2}. The selection of 100% SOC was made to enable comparison with the performance results reported in the literature.[11,13] Finally, a cycling test of 51 continuous cycles of charge-discharge was performed over the course of 16 days at a constant current density of 700 A m^{-2}, a flow rate of vanadium electrolyte of 50 mL min^{-1} and a hydrogen flow rate of 30 mL min^{-1}. The cell was allowed to return shortly to OCP before each charge or discharge step.

Additionally, averaged microstructural parameters of the vanadium electrode were obtained by imaging a sample of Freudenberg H23 carbon paper using a laboratory X-ray CT system (Phoenix Nanotom S, GE Measurement and Control, MA, USA). The Freudenberg H23 sample dimensions were 834 μm × 1585 μm × 179 μm and a resolution of 1 μm was used. Tomographic reconstruction of the acquired projection images was performed, followed by image pre-processing and segmentation of the resulting reconstructed volume that was carried out using commercial image processing software (Avizo) and an open source software (Taufactor,[32] ImageJ and Fiji). Averaged values of porosity, fiber diameter, pore diameter, and specific surface area were estimated, and are summarized in Table I. These averaged values were used in the model as material property values or bound values for the fitting parameters of the model.

Results and Discussion

The model was developed and solved in MATLAB R2017a by means of an Ordinary Differential Equation (ODE) solver, with absolute and relative tolerance set at 1×10^{-6}. The simulations were carried out in an Intel Xeon E5-1620v3, 64-bit workstation with 32 GB RAM. A cell characterization was performed using experimental data of EIS, OCP, single-cycle charge-discharge, polarization curves and cycling. The calibration of the unit cell model was developed in two stages. Firstly, the OCP data were used to calibrate the complete Nernst equation (Equation 8). Secondly, one set of experimental data of the single-cycle charge-discharge potential was used to fit selected model parameters for two flow rates of vanadium electrolyte. Simulations, using the previously fitted parameters, were run for different current densities and their results were compared to the additional experimental data sets of the single-cycle charge-discharge potential. A sensitivity analysis of the model fit was performed to study the sensitivity of the variable of interest, namely the cell potential, with respect to the selected fitting parameters. Additionally, the model was tested by running simulations of polarization curves in a wider range of current density values. The effect of material property values on the cell potential was assessed by means of a relative sensitivity factor. Finally, a simulation of the cycling test was compared to the experimental data set considering 51 continuous cycles of charge-discharge potentials.

Open circuit potential.—The relation between OCP and SOC for the RHVFC was obtained to describe the equilibrium potential. The experimental SOC of the cell (SOC_e) for each OCP step was calculated by comparing the experimental capacity increase at each galvanostatic charge or discharge step with respect to the theoretical total capacity of the solution (Q_T). Equation 17 presents the experimental SOC as a function of the initial SOC ($SOC(t_i)$), the time period ($t_f - t_i$) and the applied current (I_{appl}). The total capacity for our system was approximately 4342 A s, ($Q_T = c_V V_T n_e F$), considering the

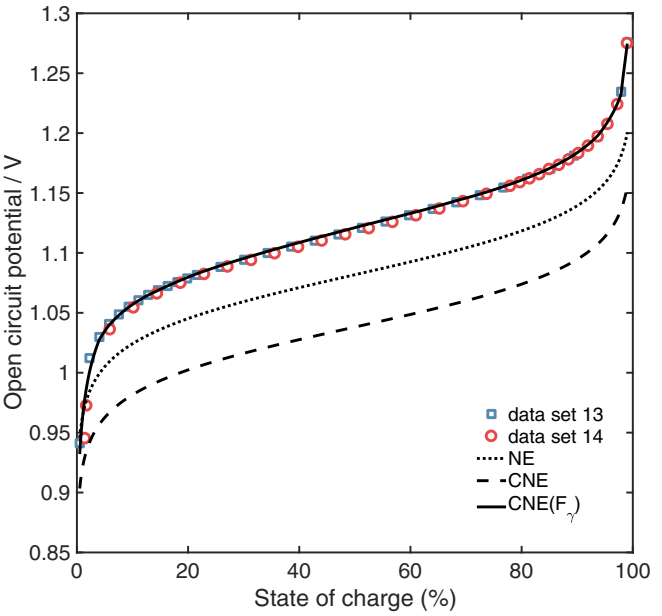

Figure 2. Comparison of experimental data of OCP with a Nernst Equation (NE), a Complete Nernst Equation (CNE) assuming unity activity coefficients for all species, and a CNE with a fitted global factor (F_γ), at a flow rate of vanadium electrolyte and hydrogen of 50 and 100 mL min^{-1}, respectively.

total volume of vanadium electrolyte in the catholyte tank (V_T), the total concentration of vanadium (c_V), and the number of electrons involved in the charge-transfer reaction (n_e). To validate the Complete Nernst Equation, Equation 8, the dependence of the concentration of species with respect to SOC is needed. The SOC of the cell can be also defined in terms of the concentration of active species as shown in Equation 17. During charge and discharge operation, changes in the concentration of all ionic species in the vanadium electrolyte occur due to the charge-transfer reaction, transport through the membrane, and acid dissociation.[17,33] The change in concentration of species was calculated by accounting for the experimental change in SOC and the dissociation of bisulphate as presented in our previous work,[17] while neglecting crossover effects. The initial concentration of all ionic species were calculated considering that the vanadium sulphate hydrate, $VOSO_4 \cdot xH_2O$, contained 3.5 molecules of water. A comparison of the estimated E_{OCP} and experimental data of OCP for the 5 cm^2 area RHVFC is presented in Figure 2.

$$SOC_e = SOC(t_i) + \frac{(t_f - t_i) I_{appl}}{Q_T}$$
$$SOC = \frac{c_{VO_2^+}}{c_{VO_2^+} + c_{VO^{2+}}} \quad [17]$$

Figure 2 shows three different equations to estimate OCP, namely a complete Nernst equation (CNE) with a fitted global factor (F_γ), a complete Nernst equation assuming unity activity coefficients for all ionic species ($F_\gamma = 1$), and a Nernst Equation (NE) that does not include the potential difference between the electrolytes (dialysis potential). The Nernst equation considerably underestimates the experimental OCP. The addition of the Donnan potential across both interfaces of the membrane acts to decrease the estimated OCP. This decrease in potential is more significant for the RHVFC than the one expected for a VRFB, since the difference of concentration of protons between cathode and anode is higher in the case of the RHVFC, e.g., about 4 M of difference. The concentration of protons in the anode of the RHVFC was considered to be equal to the fixed charge concentration in the membrane (ca., $c_f = 1.2$ M) to hold electro-neutrality, while the concentration of protons in the cathode was higher than 5 M (initial sulphuric acid concentration). A good estimation of the experimental OCP was obtained after the global factor (F_γ) was fitted. Effects

that are usually neglected when modelling the OCP of Redox Flow Batteries (RFBs), such as non-unity activity coefficients for the ionic species, were represented by this global factor. The correct estimation of the OCP is key for accurately estimating the total overpotential, which can be obtained from the difference between the measured cell potential and the estimated OCP. This total overpotential was later considered in the calibration of the fitting parameters of the model, allowing the operation of the RHVFC to be described.

Cell polarization.—*Fit of model to charge-discharge potentials.—* Experimental data of single-cycle charge-discharge potential obtained for the RHVFC with a cross-sectional electrode area of 5 cm^2 at different operating conditions of current density and flow rate of vanadium electrolyte are summarized in Table II. To calibrate the model, first the electronic conductivity for the electrodes was estimated to be of about 500 S m^{-1} and the ionic conductivity of the membrane was calculated as a function of mean water content.[17] Then, the electronic conductivity of the current collectors (σ_{cc}), including the flow fields plates, was estimated to be approximately 5000 S m^{-1}, such that the cell series resistance was consistent with the series resistance (R_s) of 0.5 Ω cm^2 obtained from the initial EIS measurements (data sets 2 and 12). This series resistance includes the effect of contact resistance. Figure 3a presents the typical EIS response of the cell represented by a Nyquist plot. EIS measurements were obtained at OCP condition with a SOC of 100% after the first galvanostatic charge of fresh vanadium electrolyte solution at a current density of 100 A m^{-2} and a flow rate of vanadium electrolyte of 100 and 50 mL min^{-1}. The total capacity measured during this first galvanostatic charge was of 4599 and 4339 A s for a flow rate of vanadium electrolyte of 100 and 50 mL min^{-1}, respectively. The series resistance corresponds to the sum of all the ohmic resistances of the cell, including electronic and ionic resistances, and also accounts for the current collectors.[11] Two depressed semi-circles are distinguished in the Nyquist plots, suggesting that at least two different processes were present when operating the cell. The high frequency process was attributed to charge transfer resistances, while the low frequency process to diffusion in the porous media. These processes could reflect contributions from both electrodes, however, considering the fast kinetics of the hydrogen electrode and the high flow stoichiometry of hydrogen used, it was reasonable to attribute the charge transfer resistance to the vanadium half-cell electrode kinetics.[11] The experimental value of the cell series resistance (0.5 Ω cm^2) was set to be a fixed parameter for all simulations. Changes in the simulated cell series resistance (R_S) were attributed to changes in the mean water content of the membrane (λ), which affects the membrane ionic conductivity[17] (σ_m), and contact resistances between cell components. During charge, transport of water through the membrane by diffusion and electro-osmotic drag occurs toward the anode, and during discharge the electro-osmotic drag flux changes direction toward the cathode while the diffusion flux maintains its direction. This change in flux direction affects the mean water content of the membrane, which presents higher values during charge than discharge operation. A higher mean water content in the membrane will increase the membrane conductivity, and therefore reduce the cell series resistance.

To quantify the relative contribution of the different processes present in the EIS response, the equivalent circuit[11] shown as an inset in Figure 3a was fitted to the EIS experimental data, considering their impedance modulus, $|Z|$, as the weighting factor. In this equivalent circuit, L represents the inductance behavior and R_S the sum of the electronic and ionic resistances of all the cell components, including current collectors. The resistance R_{CT} in parallel with the constant phase element CPE_{CT} emulates the charge transfer resistance of the vanadium redox reaction. The last element comprising of another resistance R_{Diff} in parallel with the constant phase element CPE_{Diff} was associated with the diffusion processes in the porous media. The equivalent circuit, containing the elements discussed above, was fitted with EC-lab software using a Levenberg-Marquardt algorithm. The value of the different resistance are shown in Figure 3b for the two flow rate of vanadium electrolyte used. An increase in the flow rate of vanadium

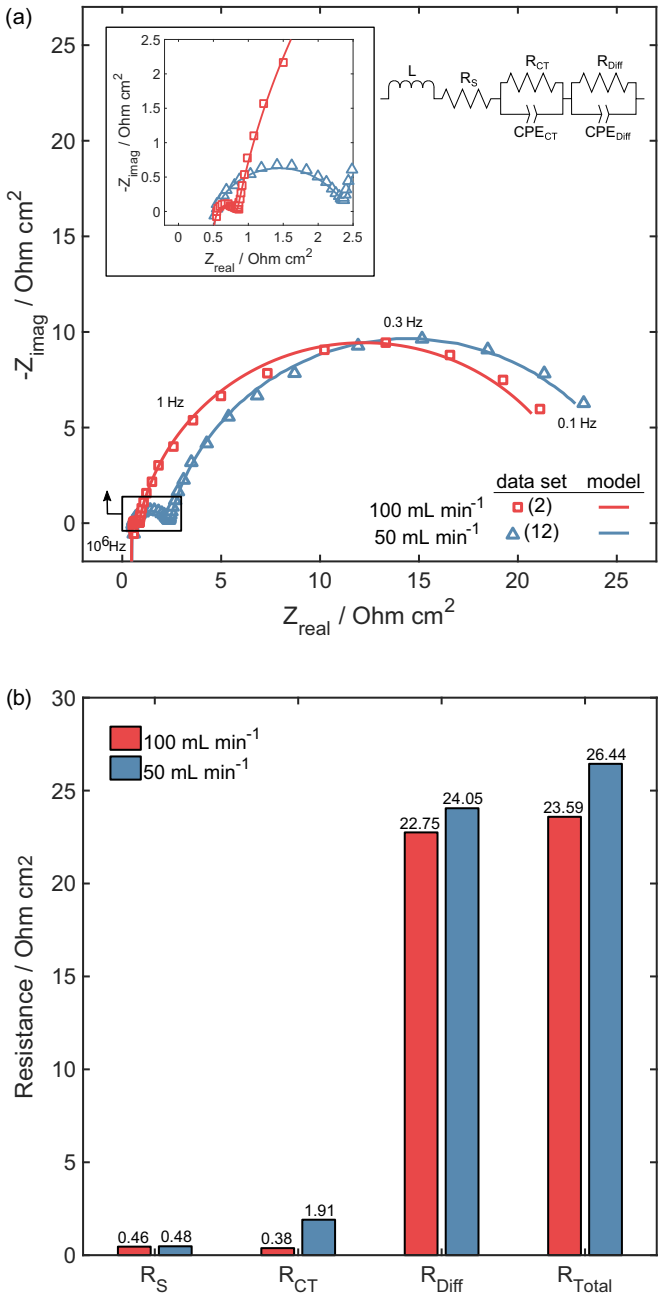

Figure 3. (a) Nyquist representation of the cell EIS response at open circuit operation with 100% of SOC, a hydrogen flow rate of 100 mL min^{-1}, and a flow rate of vanadium electrolyte of 100 and 50 mL min^{-1}; and (b) Estimated equivalent circuit parameters of resistance: series resistance (R_S), charge transfer resistance (R_{CT}), diffusion process resistance (R_{Diff}), and total cell resistance (R_{Total}).

electrolyte from 50 to 100 mL min^{-1} produced a considerable decrease of 80.1% in the charge transfer resistance (R_{CT}) and a drop of 5.4% in the diffusion related resistance (R_{Diff}). Yufit et al.[11] observed similar trends, but the change in R_{CT} (~25% at 0% SOC and ~9% at 100% SOC) when increasing the flow rate of vanadium electrolyte from 30 to 70 mL min^{-1} was not as significant as the one observed here, however a different carbon electrode for the cathode was used. Hewa Dewage et al.[9] observed an almost constant charge transfer resistance for the EIS response of the whole cell, whereas for the EIS response of the vanadium half-cell a decrease of 13% was observed when the flow rate of vanadium electrolyte was increased from 50 to 200 mL min^{-1}, also using a different cathode. In both of these works,[9,11] a cathode

Table III. Fitting parameters of the unit cell model for the 5 cm^2 area RHVFC.

Fitting parameter, θ	Symbol	Unit	Lower bound	Upper bound	Initial guess	Fitted value 100 mL min^{-1}	Fitted value 50 mL min^{-1}
Standard rate constant of cathode (θ_1)	$k_{ca,ref}$	mol m^{-2} s^{-1}	1.0×10^{-12}	1.0×10^{-6}	3.0×10^{-9}[35]	1.19×10^{-10}	4.36×10^{-11}
Active specific surface area of cathode (θ_2)	S_{ca}^{ac}	m^2 m^{-3}	1.0×10^{4}	S_{ca}^{geo}	3.0×10^{4}[36]	4.09×10^{5}	4.11×10^{5}
Cathode grouped parameter (θ_{12})	K_{ca}	mol m^{-3} s^{-1}	1.0×10^{-8}	0.429	9×10^{-5}	4.89×10^{-5}	1.79×10^{-5}
Diffusion layer thickness of cathode (θ_3)	δ^{ca}	m	1.0×10^{-6}	$3d_p^{ca}$	$d_p^{ca}/2$	1.25×10^{-5}	1.21×10^{-5}
Desorption rate constant of anode (θ_4)	$k_{des}^{\varnothing}$	mol cm^{-2} s^{-1}	1.0×10^{-7}	1.0×10^{-3}	2.1×10^{-5}[31]	2.08×10^{-5}	2.01×10^{-5}

with 5 times more cross-sectional area (25 cm^2), serpentine flow fields with higher number of flow channels (5 channels) and a higher cell compression (9 N m) was used in comparison to that used in this work. This illustrates the sensitivity of the measured performance to the electrode/cell characteristics. Further work is required to study the dependence of the charge transfer resistance on the flow rate in order to rationalize such an effect and to clarify a possible physical explanation. In this work, the series, charge transfer and diffusion resistances were used to qualitatively assist the model fitting procedure.

The calibration of the model with the cell potential was carried out against one experimental data set of a single-cycle charge-discharge potential (E_{data}) obtained during galvanostatic operation at a current density of 500 A m^{-2} for two values of flow rates of the vanadium electrolyte, 50 and 100 mL min^{-1}. An additional resistance (R), was taken into account to match the cell potential at the beginning of charge. This resistance was considered different for the operation at different flow rates of vanadium electrolyte with the value of R set to 0.94 Ω cm^2 and 0.34 Ω cm^2 for the operation at 50 and 100 mL min^{-1}, respectively. The model calibration was developed in MATLAB using a non-linear least-squares solver (lsqcurvefit function) with upper (ub) and lower (lb) bounds for the fitting parameters (θ), as shown in Equation 18. The fitting parameters were chosen to be the standard reaction rate constant of the vanadium electrode ($k_{ca,ref}$, θ_1) and the active specific surface area of the vanadium electrode (S_{ca}^{ac}, θ_2). A grouped parameter ($K_{ca} = S_{ca}^{ac} k_{ca,ref}$, θ_{12}) for the vanadium half-cell electrode is also given as electrode parameter. Also selected fitting parameters were the thickness of the Nernst diffusion layer of the vanadium electrode (δ^{ca}, θ_3), and the desorption rate constant of the Tafel reaction for the hydrogen redox reaction at standard conditions ($k_{des}^{\varnothing}$, θ_4). The grouped parameter (K_{ca}) includes the effect of the electrode kinetics and the active specific surface area of the vanadium electrode. Although, a value for the total geometric specific surface area of the vanadium electrode (S_{ca}^{geo}) was obtained by means of image analysis, its value is expected to be different to the actual value of the active specific surface area, which is related to the electrode active sites available for reaction.[34] The heat-treatment of the electrode affects the electrode kinetics as well as its total active area due to changes in the electrode wettability.[34] An alternative option would have been to set the active specific area equal to the measured specific surface area ($S_{ca}^{ac} = S_{ca}^{geo}$). A grouped parameter for the anode was not considered since the anode kinetic equation (Equations 13 to 16) is more complex and a simple substitution was not possible. Instead an assumed value was considered for the roughness factor of the anode (R_{an}) and only the desorption rate constants of the Tafel reaction at standard conditions ($k_{des}^{\varnothing}$) was varied during fitting. Upper and lower bounds were selected for each fitting parameter along with initial estimated guesses, which are summarized in Table III. It is important to mention that the fitting parameters were calibrated separately for the two flow rates of vanadium electrolyte. This decision was made based on the different EIS spectra obtained after the cell was first assembled (Figure 3), especially when considering the charge transfer process. The calibration results are presented in Figure 4, including the OCP predicted by the model by means of Equation 8. The fitted value of $k_{ca,ref}$, S_{ca}^{ac}, δ^{ca} and $k_{des}^{\varnothing}$ are summarized in Table III. A good agreement was found between experimental data and model potentials, with averaged Normalized Root-Mean-Square Error (NRMSE) of 1.2% and 13.5% for charge and discharge operation at a flow rate of vanadium electrolyte of 100 mL min^{-1}, and a NRMSE of 2.1% and 19.0% for charge and discharge operation at a flow rate of vanadium electrolyte of 50 mL min^{-1}. All NRMSEs presented in this work were normalized by the range of the measured data (y), i.e., maximum value minus minimum value ($y_{max} - y_{min}$), where y can be potential or power density.

$$\min_{\theta} \|E_{cell}(\theta) - E_{data}\|_2^2 \quad \text{subject to} \quad lb \leq \theta \leq ub \qquad [18]$$

Using the previously fitted parameters, model predictions were compared to experimental data of single-cycle charge-discharge potentials at different current densities of 100, 200, 300, 400, 1000 and 1500 A m^{-2}, and two values of the flow rate of vanadium electrolyte. Figure 5 shows the model prediction of OCP and cell potential for a current density of 300, 500 and 1000 A m^{-2} for a flow rate of vanadium electrolyte of 100 and 50 mL min^{-1}. A reasonably good agreement was found for all the current densities tested for the RHVFC model. NRMSEs for charge/discharge of 1.0/5.5% and 2.7/17.5%, 1.2/2.1% and 13.5/19.0%, and 2.4/5.3% and 16.5/10.3% were obtained for a current density of 300, 500 and 1000 A m^{-2} and a flow rate of vanadium electrolyte of 100 and 50 mL min^{-1}, respectively. The discrepancies between model predictions and experimental data were more evident at the lower flow rate of the vanadium electrolyte during discharge, and at high current densities during charge. This could be related to an increase in the mass-transport effects at the cathodic side when using a lower flow rate of vanadium electrolyte due to a decreased transport of active ionic species to and from the porous electrode. The unit cell model only incorporates the mass-transport effects within the

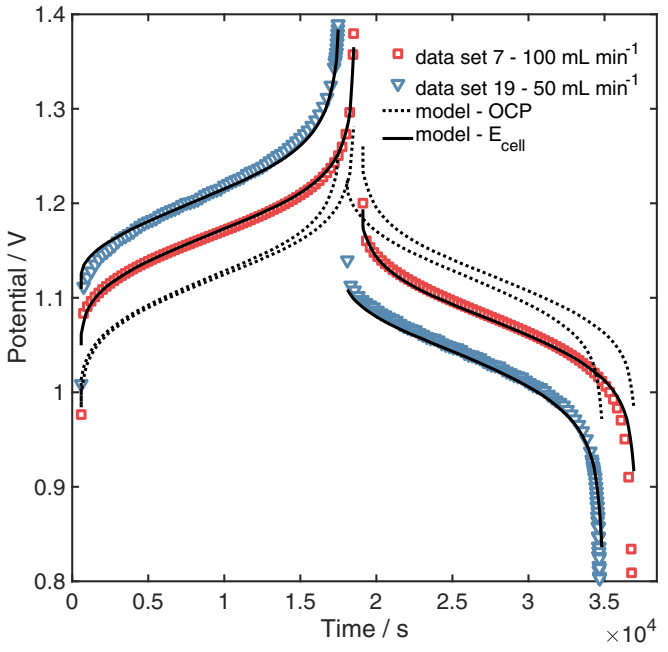

Figure 4. Calibration of model with experimental data of single-cycle charge-discharge potential at a current density of 500 A m^{-2}, a hydrogen flow rate of 100 mL min^{-1}, and a flow rate of vanadium electrolyte of 100 and 50 mL min^{-1}. OCP refers to the open circuit potential, and E_{cell} refers to the cell potential.

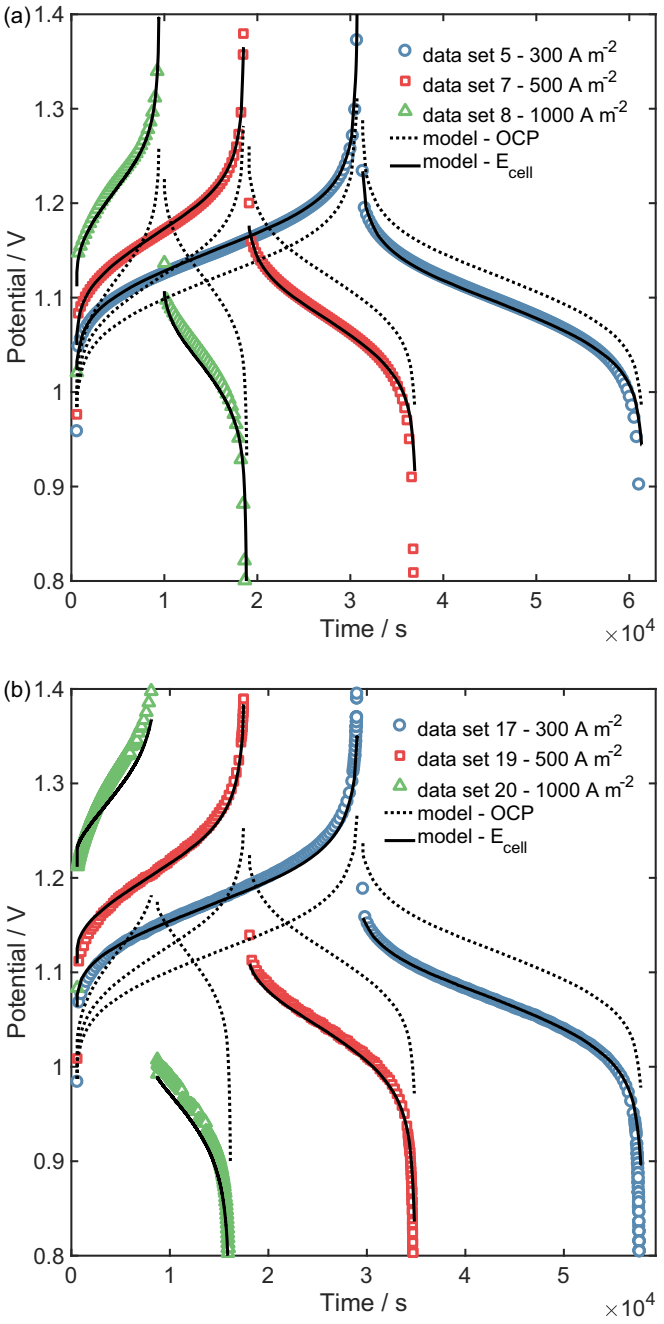

Figure 5. Comparison of experimental data of single-cycle charge-discharge potential with model testing at a current density of 300, 500 and 1000 A m^{-2} and a hydrogen flow rate of 100 mL min^{-1}. (a) flow rate of vanadium electrolyte of 100 mL min^{-1}; and (b) flow rate of vanadium electrolyte of 50 mL min^{-1}.

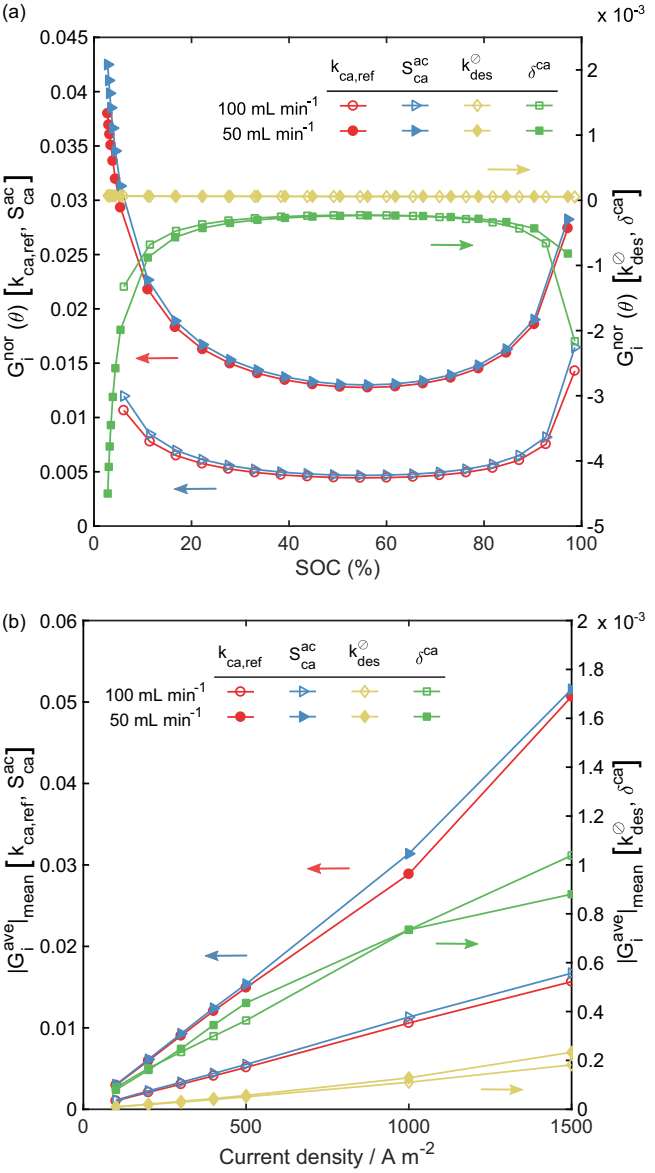

Figure 6. Model parametric sensitivity. (a) Normalized sensitivity coefficient of fitting parameters as a function of SOC during discharge operation at a current density of 500 A m^{-2}; and (b) Average absolute sensitivity of fitting parameters along variations of current density during discharge operation.

electrode pores, i.e., the difference between bulk and surface concentration, while any effect due to transport of species from the serpentine flow channel to the electrode was not accounted for in the unit cell model, which considers a zero-dimensional approach. Also, an increase in current density produces a faster depletion or generation of active species in the cathode leading to mass-transport limitation effects which were neglected in the model.

A parametric sensitivity analysis was performed considering only well fitted points of the different charge-discharge curves (data set 3 to 9 and 15 to 21).[37,38] The average absolute sensitivity of the cell potential ($|G_i^{ave}|$) with respect to the fitting parameters (θ) was assessed as a function of current density. These average absolute sensitivities were obtained considering the sensitivity coefficient (G_i) as a function of time,[38] Equation 19. Also, the normalized sensitivity coefficients (G_i^{nor}) were calculated using a central finite difference approximation after running simulations for perturbation in each fitting parameter,[37,39] Equation 20.

$$|G_i^{ave}| = \int_0^{t_{max}} \frac{|G_i(t)\theta_i / E_{cell}^{max}|}{t_{max}} dt,$$

$$G_i(t) = \frac{\partial E_{cell}(t)}{\partial \theta_i} \quad [19]$$

$$G_i^{nor}(t) = \frac{\theta_i}{E_{cell}(t)} \cdot G_i(t) = \frac{\theta_i}{E_{cell}(t)} \cdot \frac{E_{cell}(t, \theta_i + \Delta\theta_i) - E_{cell}(t, \theta_i - \Delta\theta_i)}{2\Delta\theta_i} \quad [20]$$

The G_i^{nor} coefficients describe the small change of the output cell potential, E_{cell}, with respect to the parameters, $\theta = [k_{ca,ref}, S_{ca}^{ac}, \delta^{ca}, k_{des}^{\varnothing}]$. Figure 6a presents the normalized sensitivity coefficients as a

function of SOC for the discharge potential at a current density of 500 A m^{-2} and two flow rates of vanadium electrolyte. Similar coefficients were obtained during charging. The cell potential during discharge increased with $k_{ca,ref}$, S_{ca}^{ac} and $k_{des}^{\varnothing}$, and a stronger effect was observed at the low flow rate of the vanadium electrolyte for both fitting parameters. While the cell potential during discharge decreased with δ^{ca}, and different flow rates of vanadium electrolyte presented a similar effect. At lower and higher SOCs the effect of $k_{ca,ref}$, S_{ca}^{ac} and δ^{ca} increases significantly with respect to the values at the intermediate region of SOC. These parameters are involved in the kinetic relation for the cathode (Equations 9 to 12), and a change in the parameters tends to have a higher effect in the extreme regions of SOC where the resulting overpotential is expected to be higher. As expected a faster cathodic parameter K_{ca} will produce an increase in cell potential during discharge, i.e., a lower overpotential, while a thicker diffusion layer, δ^{ca}, will cause a decrease in the cell potential during discharge, i.e., a higher overpotential. Similar results were obtained for the charging operation. Figure 6b shows the average absolute sensitivity as a function of the current density variation during discharge operation. The effect of the fitting parameters on the cell potential during discharge increased as the current density increased. The average absolute sensitivity of the cell potential varied between 3×10^{-3} and 0.052 for $k_{ca,ref}$ and S_{ca}^{ac}, 1.0×10^{-5} and 2.3×10^{-4} for $k_{des}^{\varnothing}$, and 8.0×10^{-5} and 1.0×10^{-3} for δ^{ca}. Therefore, the cell potential was consistently more sensitive to the cathodic kinetic parameters across the current density, and at high current densities δ^{ca} was more significant.

Characteristic performance features.—The performance of the RHVFC was evaluated using the experimental data of single-cycle charge-discharge potentials at different current densities. Commonly, four figures of merit are used to indicate performance of charge-discharge tests on electrochemical cells.[40–42] These figures are the coulombic, voltage, and energy efficiencies, and the electrolyte utilization (Equations 21 and 22), which are defined as:

1. Coulombic efficiency (η_C), ratio of the discharge capacity to the charge capacity.
2. Voltage efficiency (η_V), the ratio of the average discharging voltage to the average charging voltage.
3. Energy efficiency (η_E), ratio of the discharge energy to the charge energy. It is the product of the coulombic and voltage efficiencies
4. Electrolyte utilization (EU), the ratio of the actual charge or discharging capacity to the theoretical total capacity of the electrolyte.

$$\eta_C = \frac{\int_0^{t_{dis}} I_{dis}\, dt}{\int_0^{t_{ch}} I_{ch}\, dt}, \quad \eta_E = \frac{\int_0^{t_{dis}} E_{dis} I_{dis}\, dt}{\int_0^{t_{ch}} E_{ch} I_{ch}\, dt}, \quad \eta_V = \frac{\eta_E}{\eta_C} \qquad [21]$$

$$EU = \frac{\int_0^{t_{ch/dis}} I_{ch/dis}\, dt}{Q_T} \qquad [22]$$

The coulombic, energy and voltage efficiencies and the electrolyte utilization during discharge are presented in Figures 7a and 7b, respectively. The performance features of the RHVFC were consistently better at the higher flow rate of the vanadium electrolyte. The coulombic efficiencies for the 5 cm^2 area RHVFC at a flow rate of vanadium electrolyte of 100 mL min^{-1} were over 98%, with a lowest value of 98.2% at a current density of 1500 A m^{-2}. This suggests that the rate of self-discharge of the cell due to crossover of species was not important for the experimental current densities and single-cycle test times used. At the low flow rate, a moderate decrease in coulombic efficiency at high current densities was observed. This coulombic efficiency drop is related to the fact that the system displayed a mass-transport limited behavior quite early on, when using a flow rate of vanadium electrolyte of 50 mL min^{-1}. The voltage efficiency showed a virtually linear trend with respect to current density for both flow rates, decreasing as current density increased. For the high flow rate, the lowest current density of 100 A m^{-2} reached a voltage efficiency

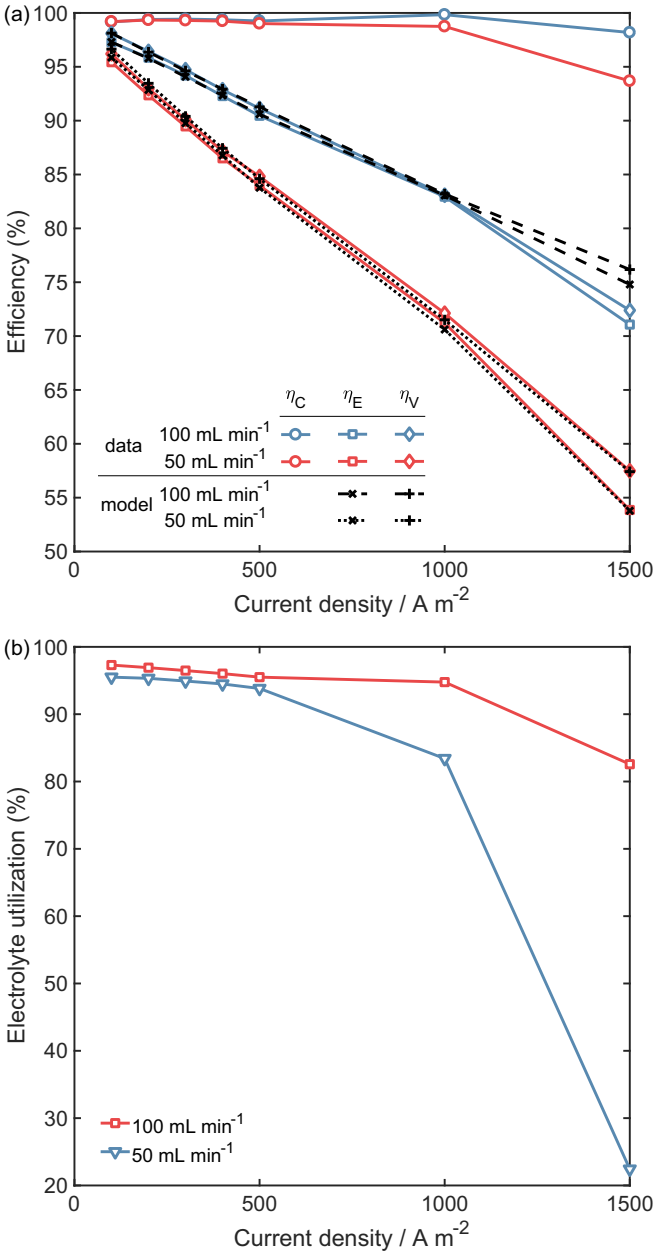

Figure 7. Figures of merit for cell tests along variations of current density at a flow rate of vanadium electrolyte of 100 and 50 mL min^{-1}, and a hydrogen flow rate of 100 mL min^{-1}. (a) Coulombic, energy and voltage efficiency during single-cycle charge-discharge operation; and (b) Experimental electrolyte utilization during discharge operation.

of 98.1%, while the highest current density of 1500 A m^{-2} resulted in a value of only 72.4%. The voltage efficiency was lower for the low flow rate of vanadium electrolyte, with a value of 57.5% at a current density of 1500 A m^{-2}. This difference in voltage efficiency tends to rise with the increase in current density. An increase in overpotential was observed in the measured potential at the low flow rate of vanadium electrolyte and at high current densities. This increased overpotential was explained by poor mass transport conditions at the cathodic side along with additional overpotentials that could appear at the anodic side. The electrolyte utilization during discharge at low current densities (<500 A m^{-2}) were very similar, with a mean value of 95.6%, for the high and low flow rates of vanadium electrolyte. A lower electrolyte utilization during discharge at a flow rate of vanadium electrolyte of 50 mL min^{-1} was also observed. For this flow

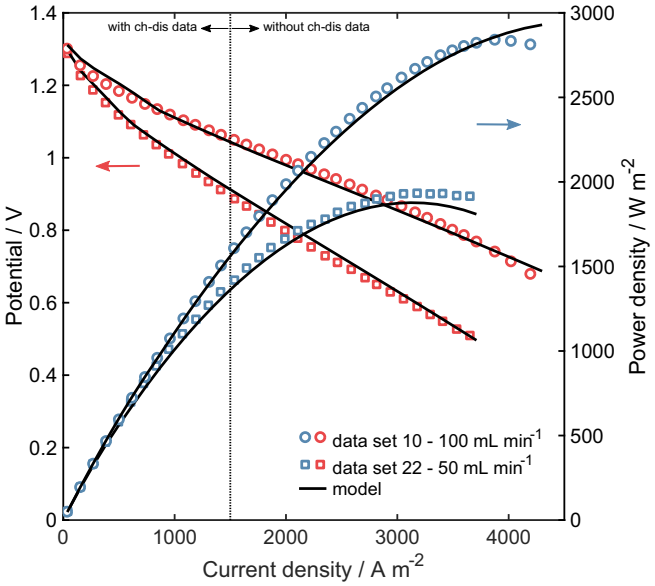

Figure 8. Comparison of model predictions with polarization data at a SOC of 100%, a flow rate of vanadium electrolyte of 50 and 100 mL min^{-1}, and a hydrogen flow rate of 100 mL min^{-1}. Two current density (j) regions: a validated region ($j \leq 1500$ A m^{-2}), where the model was fitted to charge-discharge (ch-dis) data, and a more uncertain region ($j > 1500$ A m^{-2}), where charge-discharge data were not available.

rate a minimum value of electrolyte utilization of 22.4% at a current density of 1500 A m^{-2} was observed, while the value rose to 82.6% at the higher flow rate of vanadium electrolyte of 100 mL min^{-1}. A comparison of the experimental voltage and energy efficiencies and the model predictions for all the current densities tested is also included in Figure 7a. It is worth mentioning that the operating time and current density used at each galvanostatic charge-discharge test were inputs of the models, and as such, the coulombic efficiency and electrolyte utilization matched perfectly with the experimental values obtained. The model predicted the voltage and energy efficiencies well, only showing minor discrepancies at the higher current densities.

Comparison of polarization curves.—Polarization curves of the 5 cm^2 RHVFC at a SOC of 100% are presented in Figure 8 for two flow rates of the vanadium electrolyte. During discharge at the low flow rate of 50 mL min^{-1}, mass-transport effects from around 500 A m^{-2} with a limiting current density over 3652 A m^{-2} and peak power density of 1930 W m^{-2} were observed. When a high flow rate of vanadium electrolyte of 100 mL min^{-1} was used, there was a significant increase in performance, with a peak power density of 2840 W m^{-2} and a limiting current density over 4200 A m^{-2}. This higher performance could be attributed to an improved transport of active species to and from the porous electrode. Dowd et al.[13] reported similar performance at an initial SOC of 90% with a cell configuration consisting of a carbon paper cathode, a Pt coated carbon paper anode and a N115 membrane. A peak power density of 1680 W m^{-2} at a current density of 2700 A m^{-2} and a limiting current density above 3500 A m^{-2} for a flow rate of vanadium electrolyte of 12 mL/min were reported. Model predictions of polarization curves are included in Figure 8, indicating the validated range of the current density. At high current densities, the model differed from the experimental data, displaying slightly lower performances than the ones experimentally obtained. This behavior occurred approximately from 2500 A m^{-2} at the low and high flow rates of the vanadium electrolyte. It is worth mentioning that the model was calibrated with experimental data of a single-cycle charge-discharge potential at current densities in the range of 100 to 1500 A m^{-2}. For the single-cycle charge-discharge tests only current densities up to 1500 A m^{-2} were used since for the experimental set-up employed in this work higher current densities produced lower electrolyte utilizations, which was more significant at lower flow rates of vanadium electrolyte (Figure 7b). The mismatch at high current densities could be explained by additional transport phenomena that may well have appeared during operation at high current densities. This additional phenomena could be related to anodic mass-transport limitations related to transport of water across the membrane and the anode, and crossover of ionic species. Additional data of charge-discharge operation at higher current densities (>1500 A m^{-2}) is required to study this phenomena, as well as to calibrate or modify the model for a wider range of current densities.

Effect of cell component properties.—The implementation of the unit cell model required a number of component properties, whose values were assumed as known. These properties were extracted from literature published for VRFBs and PEM fuel cells, and can be found in Table II or in our previous work.[17] Also required by the model are the operating conditions used in every experiment, such as initial concentration of vanadium and sulphuric acid species, vanadium electrolyte volume in the tank, inlet pressure of hydrogen, flow rates of vanadium electrolyte and hydrogen, temperature, and applied current density. An analysis of the influence of some of the properties (P) on the output cell potential was carried out by consecutively changing their standard value (P_i^0) by 5% and 10% to a modified value P_i^+. This change in the parameter value resulted in a relative change in the variable of interest, which in this case is the cell potential, $\partial E_{cell} = (E_{cell}^+ - E_{cell}^0)/E_{cell}^0$. A factor ($f_{rel}$) was obtained to quantify the relative sensitivity of the cell potential with respect to changes in the standard values of properties and operating conditions. This relative factor is obtained in a similar fashion to G_i^{nor}, as shown in Equation 23. A value of $f_{rel,\,i} = 1$ indicates direct proportionality between the model parameter and the simulation target.[43] This analysis can also provide guidelines to determine for which parameters an independent validation is important,[43] for example parameters with values of $f_{rel,\,i} > 0.1$. It is important to consider that in reality a change in a particular property most probably will affect the value of other properties, when considering for example microstructural properties.[44] As such, the analysis is intended as a numerical exercise to evaluate the relative importance of each individual property on the target output of the model.

$$f_{rel,\,i} = \frac{P_i}{E_{cell}(t)} \frac{\partial E_{cell}(t)}{\partial P_i} = \frac{P_i^0}{E_{cell}^0(t)} \frac{(E_{cell}^+(t) - E_{cell}^0(t))}{P_i^+ - P_i^0} \quad [23]$$

Figure 9 reports the relative sensitivity of the cell potential with respect to a relative change in the value of properties during discharge operation at a current density of 500 A^2 m^{-1}. As expected, the cell potential during discharge increased, i.e., showed a lower total overpotential, as the kinetic rate constants (k_{ca}^{ref} and $k_{des}^{\varnothing}$), the active specific area of the electrodes (S_{ca}^{ac} and R_{an}), and the component conductivities (σ_k) increased. A similar effect was observed for the cathode thickness (l_{ca}), the porosity of the cathode (ε_{ca}) and the volume fraction of polymer electrolyte in the membrane (ε_m). On the other hand, the cell potential during discharge decreased, i.e., it showed a higher total overpotential, as the porosity of the GDL (ε_{GDL}), the thickness of the membrane and GDL (l_m and l_{GDL}), and the cathodic transfer coefficient of the cathode kinetics (α_c) increased. Similarly, the cell potential during charge was affected by the properties, but in general the opposite effect was observed. Most of these trends seem obvious when considering the effect of each property in the ohmic, cathodic or anodic overpotential,[17] but interestingly only a subgroup of properties affect the potential response considerably. Among these properties the transfer coefficient of the kinetic relation for the cathode and its porosity, and the membrane thickness, have a major influence on the discharge cell potential. The effect of the porosity of the cathode is mostly related to how this property affects the effective conductivity of the cathode, while the transfer coefficient of the cathodic reaction affects the cathode overpotential response. The effect of the membrane

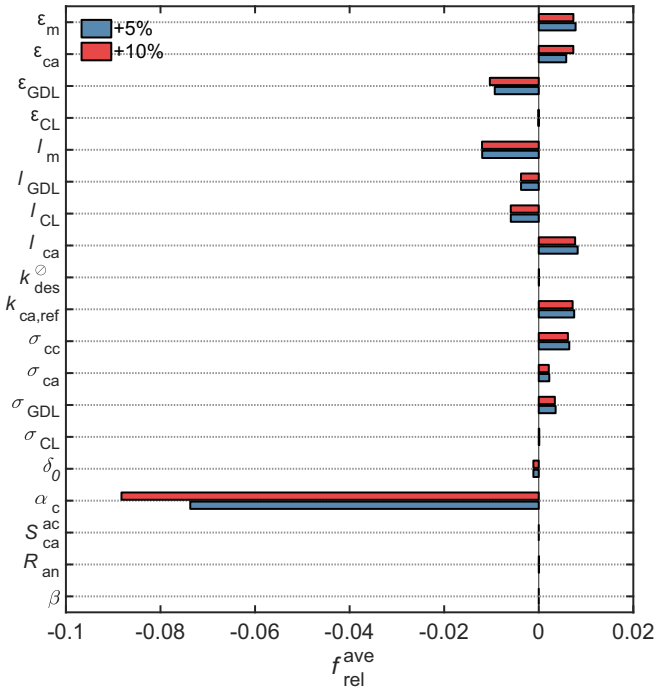

Figure 9. Average relative sensitivity of the model prediction of cell potential during discharge operation at a current density of 500 A m^{-2} with respect to a relative change of 5% and 10% of component property values.

thickness is directly related to the crossover of ionic species and water. This study suggests that care should be taken when selecting the values of porosity and transfer coefficient to reduce the uncertainty of these parameters. Thus, it is recommended to conduct a kinetic study of the relationship between current density and overpotential for the cathode, namely a Butler-Volmer relation (Equation 9), at more practical concentrations of vanadium and sulphuric acid such as the ones used in this work (0.8 M of vanadium sulphate hydrate dissolved in 5 M H_2SO_4). On the other hand, it is important to consider a more detailed description of the species and water transport through the membrane and the anode, to understant the dominant phenomena involved and its effect on the cell performance.

Cycling cell performance.—To quantify the loss of capacity and the figures of merit of the cell over continuous operation, a cycling test was performed comprising 51 continuous cycles of charge-discharge at a constant current density of 700 A m^{-2}, a flow rate of vanadium electrolyte of 50 mL min^{-1}, and a hydrogen flow rate of 30 mL min^{-1}. A short period at OCP condition before each charge and discharge was allowed for each cycle. This permitted the OCP to be tracked along the cycling test which is a qualitative estimation of the SOC of the cell when fully charged or discharged. Figure 10a presents the comparison of the experimental potential data for the cycles 2, 15, 30 and 45 and the model testing. The experimental data showed a capacity change from 4485 to 4205 A s over 51 cycles with a virtually linear trend. This total capacity change represented a capacity loss of ca. 5.6 A s per cycle or ~0.12% per cycle, which responds to crossover of vanadium (VO^{2+} and VO_2^+) and sulphuric acid (H^+, SO_4^{2-} and HSO_4^-) species, as well as liquid water, into the anodic side. During the cycling test, it was possible to observe a blueish solution slowly accumulating in the crossover reservoir connected at the hydrogen outlet, which confirmed the loss of solution to the anodic side. Figure 10a includes the model simulation of the cycling operation for the 4 cycles presented. A reasonably good agreement was found for the potential simulations, with NRMSEs for charge and discharge in the range of 1.5–12.6% and 24.8–30.4%, respectively. The main discrepancies were found at the tails of the charge and discharge potential, which is most probably related to discrepancies in the expected ionic concentrations. It was clear that a small variation in the ionic concentrations, and therefore the cell capacity, at the end of charge or discharge produced a mismatch in the cell potential. At discharge, for example, if the ionic concentrations are slightly higher, the potential does not reach the region where the potential falls rapidly, i.e., mass-transport controlled region. The opposite situation occurs if the concentrations are slightly lower toward the end of charge. In this work, the simulations were run at exactly the same operating conditions of current density and time as in the experimental operation of the cell. It is clear that if the operating time were slightly longer during the simulations, the potential would have fallen sharply as expected.

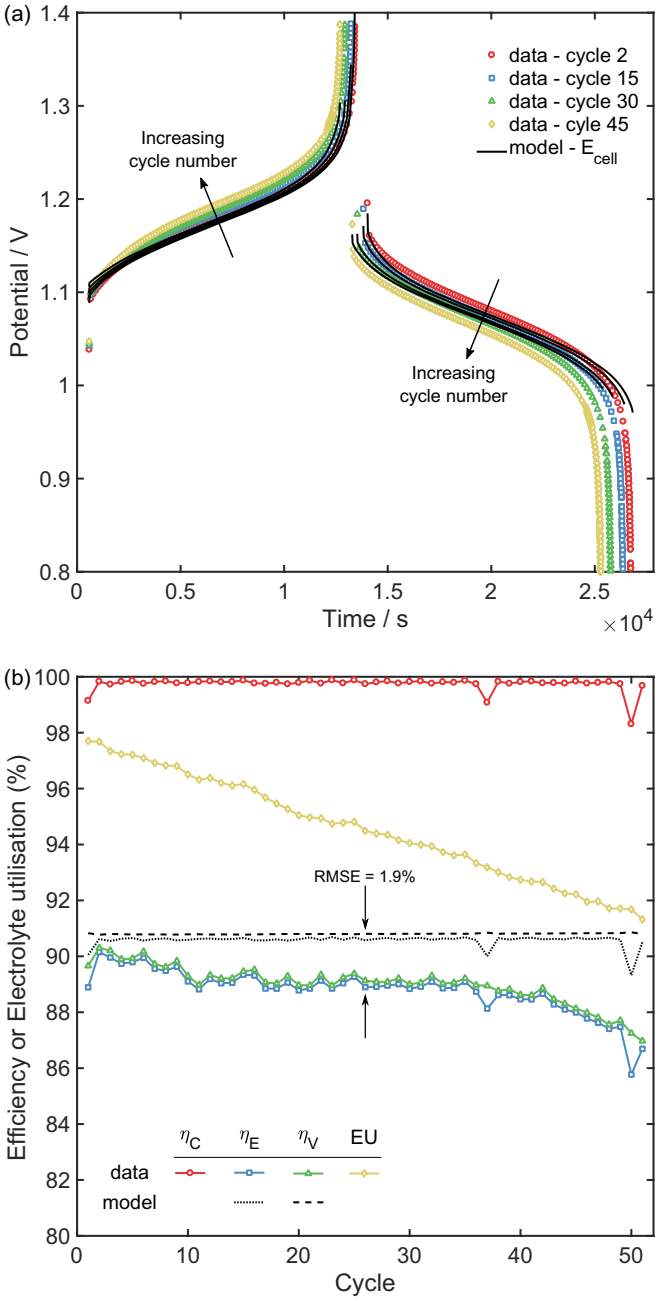

Figure 10. Cycling test at a current density of 700 A m^{-2}, a flow rate of vanadium electrolyte of 50 mL min^{-1}, and a hydrogen flow rate of 30 mL min^{-1} (data set 23). (a) Comparison of charge-discharge potential data for cycles 2, 15, 30 and 45 with model cycling test; and (b) Figures of merit for cycling test along 51 continuous cycles of charge-discharge operation.

Figure 10b shows the variation of the experimental electrolyte utilization and coulombic, energy and voltage efficiency, as defined in Equations 21 and 22, as a function of 51 continuous cycles of charge-discharge. The experimental data showed an electrolyte utilization that varied almost linearly from 97.7% to 91.3% over 51 cycles. This decrease in the electrolyte utilization is directly related to the loss in capacity due to crossover of ionic species and liquid water, as well as to an increase of cell resistances, and therefore, an increase of the total cell polarization which caused the cut-off potentials to be reached earlier than estimated. This increase in cell polarization can be observed clearly in Figure 10a. The coulombic efficiency showed a stable trend over the course of 16 days of the cycling test, with a mean value of 99.8%. It can be observed that three cycles, namely cycle 1, 37 and 50, presented a coulombic efficiency away from the mean. This was attributed to experimental anomalies during the cycling test: a noise in the current signal during the charge of cycles 37 and 50, and an initial higher potential during charge for cycle 1 due to membrane electrolyte uptake. The voltage efficiency presented a maximum and minimum value of 90.3% and 87.0%, with a slow decreasing trend over time. This decrease in voltage efficiency was also reflected in the energy efficiency and it is related to the increase of the total cell polarization. The coulombic and voltage efficiencies were slightly higher than those reported for all-vanadium systems at similar current densities (300–1000 $A^2\ m^{-1}$),[45,46] and the capacity loss was smaller for the hydrogen-vanadium system. The model estimation of voltage and energy efficiencies was higher than those expected experimentally, with a RMSE of 1.9% when considering all 51 cycles. This discrepancy is related to a slight mismatch in the concentration of species at the end of charge and discharge operation as was explained above. It is important to recognize the need for a detailed experimental and modelling study of crossover of ionic species and water, as well as possible side reactions at the anodic side, in a hybrid system such as the RHVFC. A higher-dimensional continuum model is being developed by the authors to simulate the crossover phenomena. This model will enable a better understanding of the mechanisms responsible for cell degradation through extended periods of operation, to weigh their relative importance, and to discern design strategies to improve cell performance.

To correctly describe mass-transport effects, a spatially distributed approach of a continuum or pore-level model may well be required. These distributed models could allow study of the interaction of the flow fields and the porous electrode. Such effects are out of the scope of this paper, but will be studied in the future. Additionally, an extra overpotential possibly related to mass-transport limitations has been observed in the anodic side of the RHVFC at high current densities.[47] This additional overpotential could be explained by the effect of crossover of vanadium and sulphuric acid species to the anodic catalyst layer or water management issues (flooding or drying). Moreover, Dowd et al.[12] proposed side reactions involving vanadium ionic species that could occur at the anodic side of a RHVFC. These side reactions if present will affect the performance of the cell. In order to successfully identify, quantify and describe these effects an extensive experimental study is required, as well as a detailed crossover model for a RHVFC. Further work is currently ongoing to describe the transport of water and of all ionic species across the membrane, as well as to estimate their effect on the anode performance.

Conclusions

In this study the characterization of a 5 cm^2 area RHVFC was presented, which was based on extensive experimental measurements taken at different flow rates of the vanadium electrolyte. The polarization performance of the cell had a maximum peak power density of 2840 W m^{-2} and a limiting current density over 4200 A m^{-2}, when a flow rate of vanadium electrolyte and hydrogen of 100 mL min^{-1} was used. The cycling performance of the cell displayed a capacity loss of ~5.6 A s per cycle, which was reflected in the virtually linear decrease in the discharge electrolyte utilization. This loss in capacity was related to the crossover of ionic species and liquid water into the anodic side and could also be related to possible self-discharge or side reaction involving vanadium species. The coulombic efficiency was very stable on cycling, while the voltage efficiency slowly decreased. This decrease of voltage efficiency was related to the increase in cell polarization over the 51 continuous cycles of charge-discharge.

A unit cell model including crossover of ionic species was calibrated against single-cycle charge-discharge potentials. A good agreement was found between model simulations and experimental data, while the discrepancies increased at a lower flow rate of vanadium electrolyte and at a higher current density. Simulations for polarization and power curves were obtained, with good agreement within the range of current densities validated with single-cycle charge-discharge potentials. The cell potential was more sensitive to changes in the transfer coefficient of the cathodic reaction, the cathode porosity and the membrane thickness, which are directly related to the cathodic overpotential from the Butler-Volmer equation, the cathodic ohmic overpotential, and the crossover effects. A kinetic study of the cathodic reaction is recommended at practical concentration levels, to reduce the uncertainty of the kinetic parameters such as transfer coefficients and rate constants. It is also necessary to obtain good estimations of microstructural parameters such as porosity and specific areas of electrodes. At the very least, it is important to differentiate between the geometrical specific surface area, i.e., the total area available, and the active specific surface area, i.e., a fraction of the total area that is used for the redox reaction.

It is important to highlight the need for reliable and detailed experimental data at high current densities to test and extend the range of validity of the model. Since different processes could dominate at lower or higher current densities, as well as, lower or higher SOCs, it is imperative to carry out an extensive model validation over a wider range of conditions. At the same time, this validation could help to recognize phenomena that need to be included in the model description or processes that could be neglected. Specifically, the anodic overpotential at high current densities and the effect of cross-over of vanadium and sulphuric acid species into the CL must be assessed in order to unambiguously elucidate and describe all the relevant phenomena involved in a RHVFC. Current research is focused in the formulation of a higher-dimensional continuum model that could describe the transport of ionic species and water through the membrane in a hydrogen-based hybrid RFB to improve the understanding of the crossover mechanisms and its impact on cell degradation.

Acknowledgments

The authors would like to acknowledge BECAS CHILE-CONICYT, Ministry of Education Chile Scholarship and EPSRC UK grants EP/L019469/1, EP/K002252/1, EP/L014289/1 and EP/P003494/1 for funding this work. We would like to express our appreciation to Dr. Oluwadamilola Taiwo for obtaining the characteristic micro-structural parameters of the carbon paper used for the vanadium half-cell reaction.

List of Symbols

Variables

a_i	activity of species i, –
A_k	cross-sectional area of domain k, m^2
c_i	concentration of species i, mol m^{-3}
c_V	total concentration of vanadium, mol m^{-3}
CPE	constant phase element, $\Omega^{-1}s^n$ where n is the CPE exponent.
D_i	diffusion coefficient of species i, $m^2\ s^{-1}$
d_f	mean fiber diameter, m
d_p	mean pore diameter, m
E	potential, V
E°	standard potential, V
EU	electrolyte utilization, –
F	Faraday's constant, 96485 C mol^{-1}

F_γ	global factor in the complete Nernst's equation, –
f_{rel}	relative sensitivity factor, –
G	sensitivity coefficient of fitting parameter, –
G^{ave}	average sensitivity of fitting parameter, –
I	current, A
j_0	exchange current density, A m^{-2}
j	current density, A m^{-2}
k	rate constant, mol m^{-2} s^{-1}
K	combined parameter, s^{-1}
l_k	thickness of domain k, m
L	inductance, H
n_e	number of electrons, –
N_i	molar flux of species i, mol m^{-2} s^{-1}
p_i	partial pressure of species i, Pa
P_i	property
Q_T	theoretical capacity, A s
R	universal gas constant, 8.314 J mol^{-1} K^{-1}
R_k	roughness factor of domain k, m^2 m^{-2}
R_n	resistance contribution n, Ω cm^2
S_d	dissociation reaction term, mol s^{-1}
s_k	liquid saturation of domain k, –
S_k	specific surface area of domain k, m^2 m^{-3}
SOC	state of charge, –
T	temperature, K
t	time, s
V_k	volume of domain k, m^3
v	bulk velocity, m s^{-1}
Z	impedance, Ω m^2
z_i	charge number of species i, –

Greek

α	transfer coefficient of cathode reaction, –
β	transfer coefficient of anode reaction, –
γ_i	activity coefficient of species i, –
δ	thickness of the diffusion layer, m
ε	porosity, –
η	efficiency, –; overpotential, V
θ	hydrogen coverage, –; parameters
μ_i	mobility of species i, m^2 V^{-1} s^{-1}
ξ_{drag}	electro-osmotic drag coefficient, –
σ_k	conductivity of domain k, S m^{-1}
ϕ	ionic (solution) potential, V

Superscripts and Subscripts

+	modified value
∅	standard conditions
0	initial value of variable ($t = 0$)
a	anodic
ac	active
ad	adsorption
an	anode
appl	applied
BV	Butler-Volmer
C	coulombic
c	cathodic
ca	cathode
cc	current collector
ch	charge
CL	catalyst layer
CT	charge transfer
des	desorption
Diff	Diffusion
dis	discharge
E	energy
e	experimental
eq	equilibrium
f	fixed charge; final
g	gas phase
GDL	gas diffusion layer
geo	geometric
H_{ad}	adsorbed hydrogen
i	ionic species, i= $\left[VO^{2+}, VO_2^+, H^+, HSO_4^-, SO_4^{2-}\right]$; initial
k	domain, k= [ca, an, m, CL, GDL]
m	membrane
max	maximum
n	resistance contribution, n= [S, CT, Diff]
nor	normalized
OCP	open circuit potential
ohm	ohmic
ref	reference
S	series
s	surface
T	vanadium tank
TV	Tafel-Volmer
V	Volmer; voltage
w	water

ORCID

C. A. Pino-Muñoz https://orcid.org/0000-0001-5138-4030

References

1. A. B. Gallo, J. R. Simoes-Moreira, H. K. M. Costa, M. M. Santos, and E. Moutinho dos Santos, *Renewable and Sustainable Energy Reviews*, **65**, 800 (2016).
2. L. F. Arenas, C Ponce de Leon, and F. C. Walsh, *Journal of Energy Storage*, **11**, 119 (2017).
3. M. Skyllas-Kazacos, M. H. Chakrabarti, S. A. Hajimolana, F. S. Mjalli, and M. Saleem, *Journal of The Electrochemical Society*, **158**(8), R55 (2011).
4. Z. Yang, J. Zhang, M. C. W. Kintner-Meyer, X. Lu, D. Choi, J. P. Lemmon, and J. Liu, *Chemical Reviews*, **111**(5), 3577 (2011).
5. H. Chen, T. N. Cong, W. Yang, Ch. Tan, Y. Li, and Y. Ding, *Progress in Natural Science*, **19**(3), 291 (2009).
6. P. Alotto, M. Guarnieri, and F. Moro, *Renewable and Sustainable Energy Reviews*, **29**, 325 (2014).
7. T. M. Gur, *Energy and Environmental Science*, **11**(10), 2696 (2018).
8. K. T. Cho, M. C. Tucker, and A. Z. Weber, *Energy Technology*, **4**(6), 655 (2016).
9. H. Hewa Dewage, V. Yufit, and N. P. Brandon, *Journal of The Electrochemical Society*, **163**(1), A5236 (2016).
10. M. Skyllas-Kazacos, G. Kazacos, G. Poon, and H. Verseema, *JInternational Journal of Energy Storage*, **34**, 182 (2010).
11. V. Yufit, B. Hale, M. Matian, P. Mazur, and N. P. Brandon, *Journal of The Electrochemical Society*, **160**(6), A856 (2013).
12. R. P Dowd Jr., A. Verma, Y. Li, D. Powers, R. Wycisk, P. N. Pintauro, and T. V. Nguyen, *Journal of The Electrochemical Society*, **164**(14), F1608 (2017).
13. R. P. Dowd Jr., V. S. Lakhanpal, and T. V. Nguyen, *Journal of The Electrochemical Society*, **164**(6), F564 (2017).
14. B. K. Chakrabarti, N. P. Brandon, S. A. Hajimolana, F. Tariq, V. Yufit, M. A. Hashim, M. A. Hussain, C. T. J. Low, and P. V. Aravind, *Journal of Power Sources*, **253**, 150 (2014).
15. O. Nibel, S. M. Taylor, A. Patru, E. Fabbri, L. Gubler, and T. J. Schimdt, *Journal of The Electrochemical Society*, **167**(7), A1608 (2017).
16. A. M. Pezeshki, J. T. Clement, G. M. Veith, T. A. Zawodzinski, and M. M. Mench, *Journal of Power Sources*, **295**, 333 (2015).
17. C. A. Pino Muñoz, H. Hewa Dewage, V. Yufit, and N. P. Brandon, *Journal of The Electrochemical Society*, **164**(14), F1717 (2017).
18. Q. Zheng, X. Li, Y. Cheng, G. Ning, F. Xing, and H. Zhang, *Applied energy*, **132**, 254 (2014).
19. FuelCellStore, Freudenberg gas diffusion layers for PEMFC and DMFC.
20. FuelCellStore, 0.3 mg cm^{-2} 40% Platinum on Vulcan - Carbon Paper Electrode.
21. FuelCellStore, Properties of Nafion PFSA Membrane: 115, 117 and 1110.
22. Scribner Associates, 5 cm^2 graphite flow field with REF channel.
23. R. M. Darling, A. Z. Weber, M. C. Tucker, and M. L. Perry, *Journal of the Electrochemical Society*, **163**(1), A5014 (2016).
24. J. S. Newman and K. E. Thomas-Alyea, *Electrochemical Systems*, John Wiley & Sons, Inc., New York (2004).
25. A. Tang, J. Bao, and M. Skyllas-Kazacos, *Journal of Power Sources*, **196**(24), 10737 (2011).
26. M. Pugach, M. Kondratenko, S. Briola, and A. Bischi, *Applied Energy*, **226**, 560 (2018).
27. M. Pavelka, F. Wandschneider, and P. Mazur, *Journal of Power Sources*, **293**, 400 (2015).

28. W. Xu, H. Zhang, F. Xing, H. Zhang, Y. Li, J. Cao, and X. Li, *Electrochemical Acta*, **118**, 51 (2014).
29. V. Yu and D. Chen, *Journal of Solar Energy Engineering*, **136**(2), 021005-1 (2014).
30. A. J. Bard and L. R. Faulkner, *Electrochemical Methods: Fundamentals and applications*, John Wiley & Sons, Inc, New York (2001).
31. A. R. J. Kucernak and C. M. Zalitis, *The Journal of Physical Chemistry C*, **120**(20), 10721 (2016).
32. S. J. Cooper, A. Bertei, P. R. Shearing, J. A. Kilner, and N. P. Brandon, *Software X*, **5**, 203 (2016).
33. K. W. Knehr and E. C. Kumbur, *Electrochemistry Communications*, **13**(4), 342 (2011).
34. K. J. Kim, M. Park, Y. H. Kim, S. X. Dou, and M. Skyllas-Kazacos, *Journal of Materials Chemistry A*, **3**(33), 16913 (2015).
35. K. W. Knehr, E. Agar, C. R. Dennison, A. R. Kalidindi, and E. C. Kumbur, *Journal of the Electrochemical Society*, **159**(9), A1446 (2012).
36. Y. A. Gandomi, D. S. Aaron, T. A. Zawodzinski, and M. M. Mench, *Journal of The Electrochemical Society*, **163**(1), A5188 (2016).
37. M. M. Araya, J. J. Arrieta, J. R. Perez-Correa, L. T. Biegler, and H. Jorquera, *Electronic Journal of Biotechnology*, **10**(1), (2007).
38. J. Sacher, P. Saa, M. Carcamo, J. Lopez, C. A. Gelmi, and J. R. Perez-Correa, *Electronic Journal of Biotechnology*, **14**(5), (2011).
39. F. Huerta-Perez and J. R. Perez-Correa, *Journal of the Taiwan Institute of Chemical Engineers*, **83**, 1 (2018).
40. A. Tang, J. Bao, and M. Skyllas-Kazacos, *Journal of Power Sources*, **248**, 154 (2014).
41. Q. Zheng, F. Xing, X. Li, T. Liu, Q. Lai, G. Ning, and H. Zhang, *Journal of Power Sources*, **266**, 145 (2014).
42. P. Zhao, H. Zhang, H. Zhou, J. Chen, S. Gao, and B. Yi, *Journal of Power Sources*, **162**, 1416 (2006).
43. M. Vogler, A. Bieberle-Hutter, L. Gauckler, J. Warnatz, and W. G. Bessler, *Journal of the Electrochemical Society*, **156**(5), B663 (2009).
44. A. Bertei, J. Mertens, and C. Nicolella, *Electrochemical Acta*, **146**, 151 (2014).
45. S. Kim, J. Yan, B. Schwenzer, J. Zhang, L. Li, J. Liu, Z. Yang, and M. A. Hickner, *Electrochemistry Communications*, **12**(11), 1650 (2010).
46. L. Li, S. Kim, W. Wang, M. Vijayakumar, Z. Nie, B. Chen, J. Zhang, G. Xia, J. Hu, G. Graff, J. Liu, and Z. Yang, *Advanced Energy Materials*, **1**(3), 394 (2011).
47. V. Yufit, H. Hewa Dewage, and N. P. Brandon, *ECS Conference on Electrochemical Energy Conversion & Storage with SOFC-XIV*, Scontlad, July 26-31, (2015).